

Electron and phonon dispersions of the two dimensional Holstein model: Effects of vertex and non-local corrections

J.P.Hague

Max-Planck Institut für Physik Komplexer Systeme, Dresden, Germany

Abstract. I apply the newly developed dynamical cluster approximation (DCA) to the calculation of the electron and phonon dispersions in the two dimensional Holstein model. In contrast to previous work, the DCA enables the effects of spatial fluctuations (non-local corrections) to be examined. Approximations neglecting and incorporating lowest-order vertex corrections are investigated. I calculate the phonon density of states, the renormalised phonon dispersion, the electron dispersion and electron spectral functions. I demonstrate how vertex corrections stabilise the solution, stopping a catastrophic softening of the (π, π) phonon mode. A kink in the electron dispersion is found in the normal state along the (ζ, ζ) symmetry direction in both the vertex- and non-vertex-corrected theories for low phonon frequencies, corresponding directly to the renormalised phonon frequency at the $(\pi, 0)$ point. This kink is accompanied by a sudden drop in the quasi-particle lifetime. Vertex and non-local corrections enhance the effects at large bare phonon frequencies. [PUBLISHED AS J.PHYS.:CONDENS.MATTER, **15** (2003) 2535-2550 ON 22ND APRIL 2003]

PACS numbers: 63.20.Kr, 71.10.Fd, 71.27.+a, 71.38.-k

1. Introduction

Interest in the electron-phonon problem has recently been rekindled by the discovery of large electron-phonon couplings in the cuprate superconductors and the CMR manganites [1, 2, 3]. Strong electron-phonon interactions outside the regime of traditional theories are also thought to be important in the bismuthates and in potassium doped Buckminsterfullerene superconductors [4].

One of the best known approaches to the electron-phonon problem is that of Migdal and Eliashberg [5, 6]. Migdal showed that the effects of vertex corrections and momentum on the self-energy should be negligible if the phonon frequency is much less than the Fermi energy [5]. Migdal's method was developed further by Eliashberg to investigate the superconducting state [6]. The physical content of Migdal's theorem is that there is a high probability that the most recently emitted phonon is the first phonon to be reabsorbed. This is true, provided excited states remain close to the Fermi-energy, i.e. phonon energies and couplings are small compared with the band width. Within Migdal theory, it is therefore acceptable to neglect processes in which the order of emission and reabsorption is changed. When these techniques were introduced, no materials had been found where the electron-phonon coupling was strong, and the phonon frequency large compared to the Fermi energy. For this

reason, the application of Migdal–Eliashberg (ME) theory was very successful, and remains highly regarded. Unfortunately, strong electron-phonon coupling and large phonon frequencies in the systems detailed in the first paragraph is likely to make them incompatible with the Migdal–Eliashberg approach, and further extensions to the theory seem necessary. The aim of this paper is to evaluate and discuss the effects of both vertex corrections and non-local fluctuations due to the DCA on the theory of coupled electron-phonon systems.

Previous attempts to extend ME theory include the introduction of vertex corrections into the Eliashberg equations by Grabowski and Sham [7], and an expansion to higher order in the Migdal parameter by Kostur and Mitrović in order to investigate the 2D electron-phonon problem [8]. Grimaldi *et al.* generalised the Eliashberg equations to include momentum dependence and vertex corrections [9]. A discussion of the applicability of these and other approximations to the vertex function can be found in reference [10].

The importance of vertex corrections to electron-phonon problems within the local or dynamical mean-field approximation (DMFA), has been investigated by Miller *et al.* [11] and Deppeler *et al.* [12]. In these studies, the effects of both electrons on phonons and phonons on electrons are treated with equal importance, leading to a fully self-consistent theory. Miller *et al.* focus on situations where the effects of vertex corrections can be handled using a Coulomb pseudopotential extension to the basic ME theory, and where the explicit treatment of the vertex is essential. Deppeler *et al.* take the expansion to third order in the self-energy. The authors calculate physical observables, such as isotope coefficients, phonon spectral functions and superconducting transition temperatures.

The current paper goes beyond the previous work by introducing a fully self-consistent momentum-dependent self-energy to the problem via the dynamical-cluster approximation (DCA). DCA is a new technique, which extends the DMFA by introducing short-range fluctuations in a controlled manner [13]. I apply the DCA to the calculation of electron and phonon dispersion curves in the Holstein model, which is one of the simplest non-trivial models of electron-phonon systems. Two approximations for the electron and phonon self energies are applied. The first neglects vertex corrections, but incorporates non-local fluctuations. The second incorporates lowest order vertex and non-local corrections. The vertex corrections allow the sequence of phonon absorption and emission to be reordered once, and therefore introduce exchange effects. At each stage, the DCA result is compared to the corresponding DMFA result. In principle, with parameters close to the Migdal regime, this enhancement of ME theory should be sufficient to correct the results, and the series allowing for additional reorderings should be convergent. However, such an approach may not work when the phonon frequency greatly exceeds the Fermi-energy, known as the instantaneous limit.

This paper is organised as follows. In section 2, the DCA is introduced. In section 3 the Holstein model of electron-phonon interactions is described, and the perturbation theory and the full algorithm used in this work are detailed. In section 4 the results are presented. They are divided into two parts. First the effects of non-local and vertex corrections on the phonon density of states and renormalised phonon frequency are discussed. Then the electron dispersion and spectral function are computed. A summary of the major findings of this research is given in section 5.

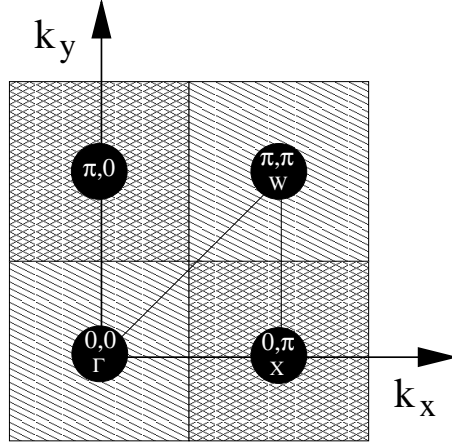


Figure 1. A schematic representation of the reciprocal-space coarse graining scheme for a 4 site DCA. Within the shaded areas, the self-energy is assumed to be constant. There is a many to one mapping from the crosshatched areas to the points at the centre of those areas. The coarse graining procedure corresponds to the mapping to a periodic cluster in real space, with spatial extent $N_c^{1/D}$. Also shown are the high symmetry points Γ , W and X , and lines connecting the high symmetry points. Since an infinite number of \mathbf{k} states are involved in the many to one mapping, the approximation is in the thermodynamic limit. The DMFA corresponds to $N_C = 1$.

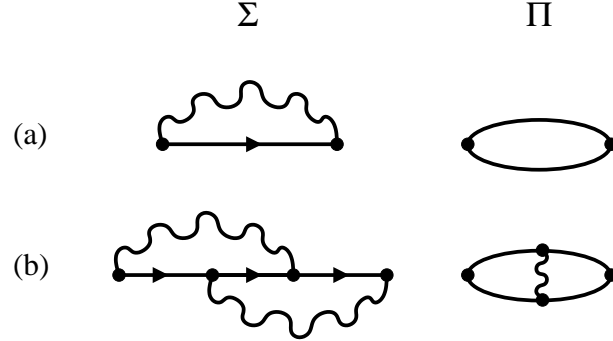


Figure 2. Diagrammatic representation of the current approximation. Series (a) represents the vertex-neglected theory which corresponds to the Migdal-Eliashberg approach. This is valid when there is a high probability that the last emitted phonon is the first to be reabsorbed, which is true if the phonon energy ω_0 and electron-phonon coupling U are small compared to the Fermi energy. Series (b) represents additional diagrams for the vertex corrected theory. The inclusion of the lowest order vertex correction allows the order of absorption and emission of phonons to be swapped once. In principle, for moderate phonon frequency and electron-phonon coupling, these additions to the theory should be sufficient to correct the results of the vertex-neglected theory. The phonon self energies are labelled with Π , and Σ denotes the electron self-energies. Lines represent the full electron Green's function and wavy lines the full phonon Green's function.

2. The dynamical cluster approximation

The dynamical cluster approximation [13, 14] is a recent extension to the dynamical mean-field approximation. DMFA has been extensively applied to solving infinite-dimensional lattice models, where the DMFA formalism becomes exact [15, 16]. It has also been used to approximate two and three dimensional systems, where it is known as the local approximation [17, 11]. In DMFA, the self-energy is assumed to be local, and $\Sigma(\mathbf{k}, z)$ is replaced by its momentum-independent counterpart, $\Sigma(z)$. As such, the Green's function may be coarse grained across the Brillouin zone,

$$G(z) = \int_{-\infty}^{\infty} \frac{\mathcal{D}(\epsilon) d\epsilon}{z + \mu - \epsilon - \Sigma(z)} \quad (1)$$

where $\mathcal{D}(\epsilon)$ is the non-interacting Fermion density of states (DOS). The chemical potential is represented by μ , and z may take the values $i\omega_n$ or $\omega + i\eta$ depending on whether one wants to work with the Matsubara or real axis Green's function (η is a small value).

Application of the DMFA to one and two dimensional models is expected to give an incomplete description of the physics. The DMFA can be thought of as the first term of an expansion in $1/n_{\text{nn}}$, where n_{nn} is the coordination number [16]. For three dimensional systems, n_{nn} ranges between 6 and 12, and it is often argued that additional terms give a minor correction. In contrast, additional terms in the $1/n_{\text{nn}}$ expansion are expected to be important in 1 and 2 dimensions. An example of significant differences between the one, two and three dimensional cases comes from isotropic-exchange spin-systems. In 3D, a finite transition temperature is found, consistent with the mean-field result (although the critical exponent is modified). However, significant non-local fluctuations in one and two dimensions are expected to reduce the Néel temperature to zero (Mermin–Wagner theorem), and the mean-field approach fails completely.

The DCA follows a similar procedure to the DMFA. The Brillouin zone is divided up into N_C subzones consistent with the lattice symmetry (see figure 1). Within each of these zones, the self-energy is assumed to be momentum independent. This leads to the relation,

$$G(\mathbf{K}_i, z) = \int_{-\infty}^{\infty} \frac{\mathcal{D}_i(\epsilon) d\epsilon}{z + \mu - \epsilon - \Sigma(\mathbf{K}_i, z)} \quad (2)$$

where $\mathcal{D}_i(\epsilon)$ is the non-interacting Fermion density of states for subzone i . The \mathbf{K}_i are the average \mathbf{k} for each subzone, plotted as the large dots in figure 1. This partial treatment of momentum dependence in the theory introduces non-local fluctuations with a characteristic length scale of $N_C^{1/D}$.

The combination of the self-energy and the coarse grained Green's function leads to a modified Dyson equation,

$$\mathcal{G}_0^{-1}(\mathbf{K}_i, z) - G^{-1}(\mathbf{K}_i, z) = \Sigma(\mathbf{K}_i, z) \quad (3)$$

The self-consistent condition is closed by calculating the self-energy from $\mathcal{G}_0(z, \mathbf{K})$, which has the interpretation of the host Green's function of a cluster impurity model (sometimes known as the cluster excluded Green's function). Different approximations exist for the calculation of the self-energy, including quantum Monte-Carlo and perturbative approaches.

Both dynamical-mean-field and dynamical-cluster approximations are calculated in the thermodynamic limit, as opposed to conventional finite sized techniques where

the particle number is equivalent to the cluster size. In this work, the DCA is used, since it involves only a small amount of additional computing time per iteration, while rapid convergence in cluster size is expected. Estimates based on the convergence of the Hubbard problem (which has a relatively strong momentum dependence) suggest that the Hubbard model is well approximated by a cluster size of $N_C = 64$ [18].

There are a number of methods that can be applied to speed up the DCA algorithm. Firstly, the symmetry of the problem may be taken into account through the appropriate *planar* point group *pm3m* [19]. In the large cluster limit, this means that only 1/8th of the total momentum points need to be used in the calculation. Similar considerations can be used to dramatically reduce the number of terms in the momentum summations needed to calculate the self-energy terms. This is particularly important when vertex corrections are included, since the calculation scales as N^3 . The Matsubara frequency sums are, in principle, infinite. However, in this work they were truncated at a frequency where asymptotic behaviour is obeyed to a certain accuracy. All points above this frequency which were needed in the calculation of another quantity were computed from the asymptotic function, ensuring an accurate self-consistent procedure. The partial DOS are central to the DCA and were calculated using the analytic tetrahedron method to ensure very high accuracy [20]. All code used in this study was written in object oriented c++ to make the implementation as simple and reliable as possible.

3. The Holstein model

A simple, yet non-trivial, model of electron-phonon interactions treats phonons as individual nuclei vibrating in a static harmonic potential (representing the interaction between all nuclei) i.e. only one frequency ω_0 is considered. The phonons couple to the local electron density via a simple momentum-independent coupling constant g . The resulting *Holstein Hamiltonian* [21] is written as,

$$H = - \sum_{ij\sigma} t_{<ij>\sigma} c_{i\sigma}^\dagger c_{j\sigma} + \sum_{i\sigma} n_{i\sigma} (gr_i - \mu) + \sum_i \left(\frac{M\omega_0^2 r_i^2}{2} + \frac{p_i^2}{2M} \right) \quad (4)$$

The first term in this Hamiltonian represents a tight binding model with hopping parameter t . Its Fourier transform takes the form $\epsilon_k = -2t \sum_{i=1}^D \cos(k_i)$. The second term connects the local ion displacement, x_i to the local electron density. Finally the last term can be identified as the bare phonon Hamiltonian. The creation and annihilation of electrons is represented by $c_i^\dagger(c_i)$, p_i is the ion momentum and M the ion mass

It is possible to find an expression for the effective interaction between electrons by integrating out phonon degrees of freedom [22]. In Matsubara space, this interaction is:

$$U(i\omega_s) = \frac{U\omega_0^2}{\omega_s^2 + \omega_0^2} \quad (5)$$

Here, $\omega_s = 2\pi sT$ are the Matsubara frequencies for bosons and s is an integer. A variable $U = -g^2/M\omega_0^2$ is defined to represent the magnitude of the effective electron-electron coupling in the remainder of this paper.

Interaction (5) has two important limits. When $\omega_0 \rightarrow 0$, the interaction is defined by a Kronecker δ function. The DMFA of this limit was written down by Freericks *et al.*, and solved by Millis *et al.* [4, 23]. When phonon frequency and coupling are

small, Migdal's theorem applies. Migdal's approach allows vertex corrections to be neglected, and results in a momentum-independent theory corresponding to a local or dynamical mean-field solution. The theorem is exact when $U = 0^-$, $\omega_0 = 0^+$.

In the limit that $\omega_0 \rightarrow \infty$, the Holstein model maps onto an attractive Hubbard model. A particular feature of this mapping is that the second order direct and exchange diagrams of the expansion in the bare propagator develop the same functional form, and are of the same order of magnitude, while the first-order diagram becomes constant and can be absorbed into the chemical potential. Since the exchange diagram includes one vertex correction, it is clear that vertex corrections are extremely important in this limit. The vertex-corrected theory described in this paper has the appropriate weak coupling behaviour for large ω_0 , unlike the vertex-neglected theory.

In this paper, the perturbation theory shown in figure 2 is used, following directly from the free energy expansion of Baym and Kadanoff [11]. The electron self-energy has two terms, $\Sigma_{\text{ME}}(\omega, \mathbf{K})$ neglects vertex corrections (figure 2(a)), and $\Sigma_{\text{VC}}(\omega, \mathbf{K})$ corresponds to the vertex corrected case (figure 2(b)). $\Pi_{\text{ME}}(\omega, \mathbf{K})$ and $\Pi_{\text{VC}}(\omega, \mathbf{K})$ correspond to the equivalent phonon self energies. The diagrams translate as follows (note that in the following 4 equations, $\mathbf{Q} \equiv (i\omega_n, \mathbf{Q})$)

$$\Sigma_{\text{ME}}(\mathbf{K}) = UT \sum_{\mathbf{Q}} G(\mathbf{Q}) D(\mathbf{K} - \mathbf{Q}) \quad (6)$$

$$\Pi_{\text{ME}}(\mathbf{K}) = -2UT \sum_{\mathbf{Q}} G(\mathbf{Q}) G(\mathbf{K} + \mathbf{Q}) \quad (7)$$

$$\Sigma_{\text{VC}}(\mathbf{K}) = (UT)^2 \sum_{\mathbf{Q}_1, \mathbf{Q}_2} G(\mathbf{Q}_1) G(\mathbf{Q}_2) G(\mathbf{K} - \mathbf{Q}_1 - \mathbf{Q}_2) D(\mathbf{K} - \mathbf{Q}_1) D(\mathbf{Q}_2 - \mathbf{Q}_1) \quad (8)$$

$$\Pi_{\text{VC}}(\mathbf{K}) = -(UT)^2 \sum_{\mathbf{Q}_1, \mathbf{Q}_2} G(\mathbf{K}) G(\mathbf{Q}_1) G(\mathbf{Q}_2) G(\mathbf{K} - \mathbf{Q}_1 + \mathbf{Q}_2) D(\mathbf{Q}_2 - \mathbf{Q}_1) \quad (9)$$

The phonon propagator $D(z, \mathbf{K})$ is calculated from,

$$D(i\omega_s, \mathbf{K}) = \frac{\omega_0^2}{\omega_s^2 + \omega_0^2 - \Pi(i\omega_s, \mathbf{K})} \quad (10)$$

and the Green's function from equation (2) $\Sigma = \Sigma_{\text{ME}} + \Sigma_{\text{VC}}$. It is possible to extend equation 10 to deal with a momentum dependent bare phonon dispersion, using a generalisation of the DMFA method in [24]. When extending the formalism to investigate a momentum-dependent interaction term, the interaction term should be coarse grained as in [14]. All the ingredients now exist for the self-consistent loop. The algorithm is started with $\Sigma, \Pi = 0$, then the DCA propagators, G and D are calculated from equations (10) and (2). Π is then calculated followed by D and Σ . The loop is completed by calculating G .

The double three-fold integration over momentum is the main barrier to performing vertex-corrected calculations, meaning that only relatively small clusters can be treated. Since the traditional phonon problem with $\omega_0, U \ll W$ (W is the bandwidth) has fluctuations which are almost momentum independent [5], it is expected that the DCA will have especially fast convergence in N_C for the parameter regime where $\omega_0, U < W$, and that calculations with relatively small cluster size accurately reflect the physics. In this respect, finite size calculations are likely to fail, and the application of DCA to this problem is essential.

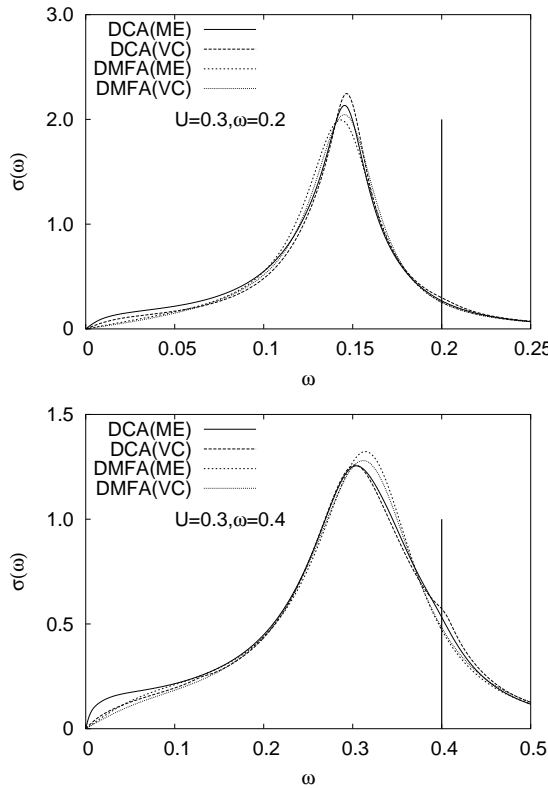


Figure 3. The renormalised phonon DOS. The upper panel gives results for $\omega_0 = 0.2$, and the lower panel for $\omega_0 = 0.4$. All four approximations are shown on each panel. The vertical line represents the δ -function characteristic of the non-interacting DOS in both cases. The effect of electron phonon coupling is to shift spectral weight to lower frequencies, and to broaden the distribution, corresponding to a finite quasi-particle lifetime. Both panels show similar behaviour, but the effects are more pronounced for $\omega_0 = 0.4$. The DMFA results show a simple distribution with a peak at the renormalised phonon frequency. Inclusion of vertex corrections in the DMFA leads to a reduction in the renormalisation, but the distribution remains similar. The inclusion of non-local corrections to the vertex-neglected theory causes an additional shift in the weight to very low frequencies. This shift is significant, because it causes a large increase in the renormalised electron-phonon coupling constant. The introduction of vertex corrections to the non-local theory causes the distribution to return to something similar to the original Migdal–Eliashberg result. This shows the importance of vertex corrections in stabilising the Migdal–Eliashberg theory.

4. Results

4.1. Phonon dispersion and DOS

In this section, the phonon DOS and renormalised phonon frequency are calculated. A moderate coupling of $U = 0.3$ was chosen, corresponding to approximately one third of the band width $W = 1$ (i.e. U is slightly larger than $t = 0.25$). Two phonon frequencies of $\omega_0 = 0.2$ and $\omega_0 = 0.4$ were chosen to demonstrate behaviour in the region where Migdal’s theorem is (or ought to be) applicable, and behaviour in the region where

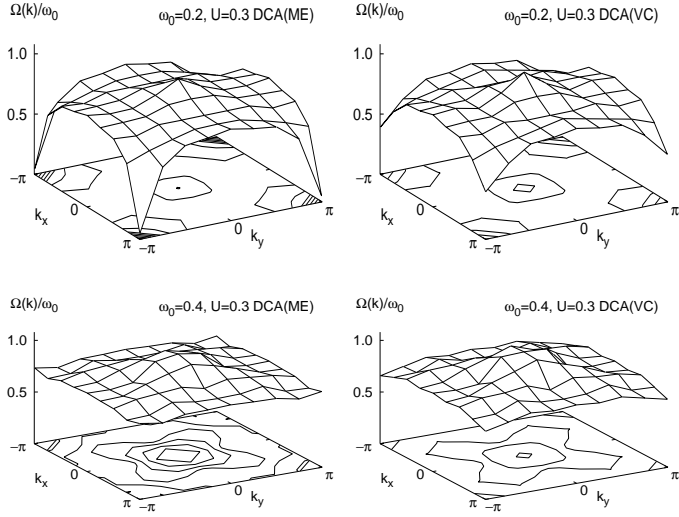


Figure 4. Renormalised phonon dispersion for the DCA. The solution from the DMFA results in a flat dispersion, and is therefore not shown here. The top row shows results for $\omega_0 = 0.2$, and the bottom row for $\omega_0 = 0.4$. Vertex neglected results are shown on the left hand side, and vertex corrected results on the right. As discussed in the text, the vertex corrections act to reduce the renormalisation of the phonon frequency. This can be seen to greatest effect in the $\omega_0 = 0.2$ results, where the fully softened point in the vertex-neglected theory is no longer fully softened in the vertex corrected theory. The dispersion is relatively flat for the $\omega_0 = 0.4$ case, which is reasonable since one expects a non-renormalised dispersion as one approaches the Hubbard limit ($\omega_0 \rightarrow \infty$).

vertex corrections are important. Computations were carried out with $N_C = 1$ and $N_C = 64$ in order to make comparisons between the DMFA and DCA result, with an additional computation for $N_C = 16$ in order to check convergence in cluster size. Although the results are not shown here, the $N_C = 16$ calculation was already close to convergence. A cutoff of 200 Matsubara points was used at a temperature of $T = 0.02$. The vertex neglected theory was calculated first, by iterating until convergence of 1 part in 10^5 . The vertex corrections were then switched on, and iteration was continued until the required accuracy was reached.

The total (momentum integrated) phonon density of states ($\sigma(\omega) = \text{Im}[D(\omega)]/\pi$) may be seen in figure 3. Since it is difficult to choose a default model for the maximum entropy analytic continuation of Bosonic propagators [25], the analytic continuation in this subsection was carried out using the Padé approximant method of Vidberg and Serene [26]. I also computed some results on the real axis for the vertex-neglected theory, and found no significant differences.

The top panel in figure 3 shows results for $\omega_0 = 0.2$, and the bottom panel for $\omega_0 = 0.4$. On each panel, results for all the approximations are shown to facilitate comparison (as is the case for most graphs in this section, exceptions will be noted with reasons). As is well documented for Migdal–Eliashberg theory, the effect of electron-phonon coupling is to shift spectral weight to lower frequencies, with the effect that the phonon frequency is renormalised to a smaller value (i.e. the phonon mode softens).

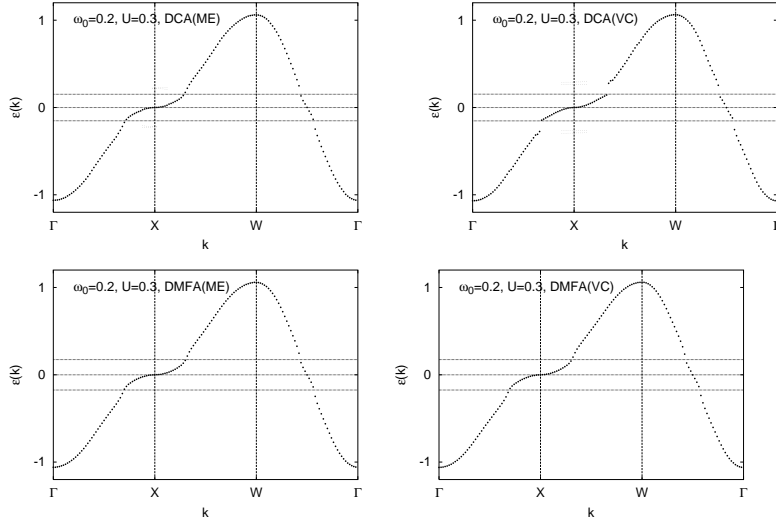


Figure 5. Electron dispersion of the Holstein model, shown for $U = 0.3$, $\omega_0 = 0.2$. Calculations for the DMFA and DCA with and without vertex corrections are shown. Note how the vertex corrections stabilise the kink. Some spurious dispersion is seen, and can be confirmed by looking at the spectral functions in figure (7). However the weighting of these points is small, and they are marked with small dots for completeness. All four approximations show a kink at the renormalised phonon energy at the $(\pi, 0)$ point (the horizontal dotted line). The kink is especially well defined along the $W\text{-}\Gamma$ line, where the 4 approaches agree to reasonable accuracy. It is possible that the kink is slightly below the phonon frequency for the DMFA calculations. A slight discrepancy is reasonable, since the renormalisation of the phonon frequency in DMFA is constant across the Brillouin zone. The kink is not well defined along the $\Gamma\text{-}X\text{-}W$ direction, except for the DCA(VC) calculations, where a sudden discontinuity is seen. The point of this discontinuity does not coincide with a boundary to the coarse grained cell, so it is expected that it is not spurious.

By way of comparison, the thick vertical line represents the δ -function characteristic of the bare phonon DOS.

The inclusion of vertex corrections into the DMFA calculation reduces the softening effect. This can be seen in both panels. The reduction in renormalisation occurs because the sign of Π_{VC} is opposite to that of Π_{ME} , i.e. the effect of particle exchange is to reduce correlation effects.

The consequences of non-local corrections to the vertex-neglected theory are also shown in the figure. The effects are significant, since a proportion of the phonon spectral weight is shifted to very low energies. As the phonon frequency is increased, the relative size of the missing vertex corrections also increases. Therefore, the number of low frequency states rises. This very low energy behaviour is extremely important, since the small parameter for the Migdal–Eliashberg perturbation theory is normally written as $\lambda = 2g^2 \int_0^\infty \sigma(\omega) d\omega / \omega$ [27]. λ is therefore significantly enhanced by the low energy modes, especially since the DOS at low energy has negative curvature. Examination of the partial phonon DOS for each coarse graining cell quickly shows that the main culprit is the (π, π) cell, which is fully softened.

Vertex corrections to the non-local theory significantly reduce the renormalisation of the (π, π) point, causing the DOS to appear similar to that calculated from the local

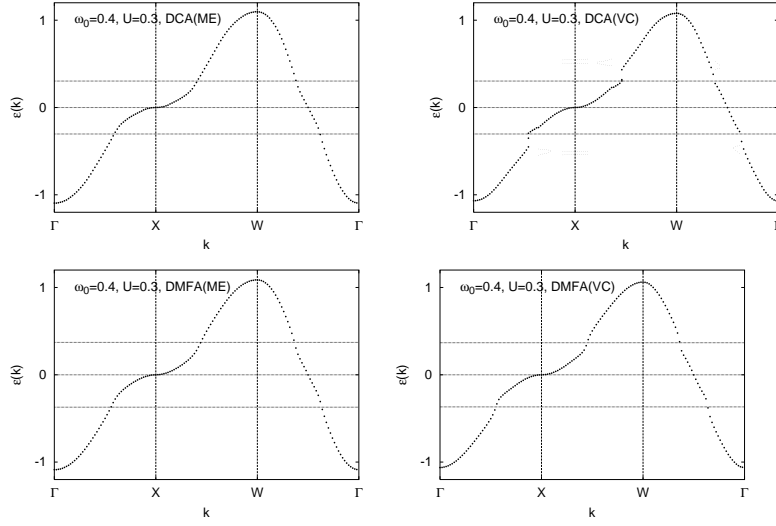


Figure 6. As figure 5 but with $U = 0.3$, $\omega_0 = 0.4$. As before, vertex corrections stabilise the kink. Some spurious dispersion is seen, and can be confirmed by looking at the spectral functions in figure (7). The weighting of the spurious points is small, but they are marked with small points for completeness. Note that the kink energy is significantly lower than the appropriate renormalised phonon frequency at the $(\pi, 0)$ point for both of the DMFA calculations. The DCA(ME) dispersion bends smoothly (rather than showing a sudden kink), at an energy which is slightly lower than the phonon frequency. The DCA(VC) has kink behaviour along the W - Γ line in contrast to the other 3 approximations. Discontinuity in the dispersion along the Γ - X - W line can also be seen at this frequency.

approximation. One expects this result, since the softening of the (π, π) mode increases the total magnitude of the vertex corrections within an iteration (by increasing the coupling constant λ) reducing λ over subsequent iterations. The phonon DOS finds an equilibrium between the softening of the vertex-neglected term and the effects of vertex corrections. This is consistent with experiments, where no full softening of the phonon frequency at the (π, π) point is observed for systems of optic phonons [3, 28]. The effects of higher order vertex corrections are expected to be consistently smaller and smaller for this parameter range, since the lowest order vertex corrections were sufficient to stabilise λ to a small value. Such an effect would presumably be irrelevant to systems of acoustic phonons, where the zone-centre mode is already zero.

In order to elucidate the deficiencies in the vertex-neglected theory more completely, the renormalised phonon frequency in a coarse grained cell, $\Omega(\mathbf{K})$, may be calculated by solving the equation,

$$\omega_0^2 - \omega^2 - \omega_0^2 \text{Re}[\Pi(\omega, \mathbf{K})] = 0 \quad (11)$$

In figure 4, surface plots showing the renormalised phonon dispersion across the whole Brillouin zone are presented. Contours are plotted beneath the dispersion to highlight the resulting symmetry. Since the DMFA and bare phonon dispersion in the model are momentum independent, the renormalised phonon dispersion relating to the DMFA calculation of the Holstein model is constant across the Brillouin zone, and is therefore not shown. In a more realistic model, the dynamical effects of the coupling between

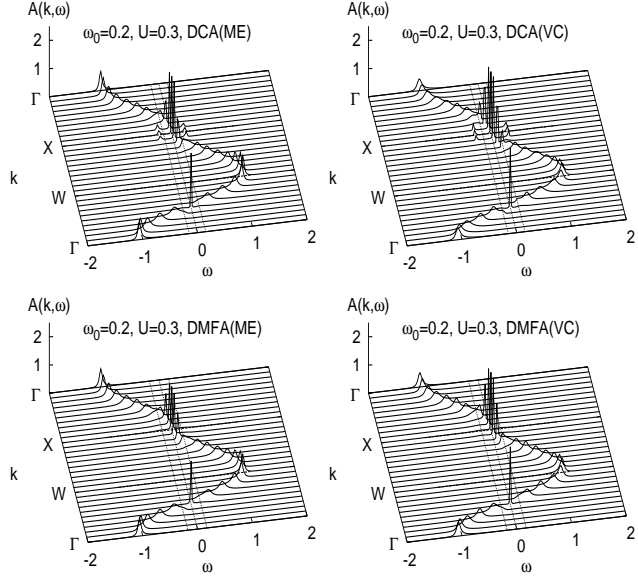


Figure 7. Spectral functions along the high symmetry directions for $U = 0.3$, $\omega_0 = 0.2$. Sharply peaked points close to the Fermi-energy ($\omega = 0$) show well defined quasi-particles. These particles are suddenly damped at the renormalised phonon energy of the $(\pi, 0)$ point (parallel dotted lines). However, at higher frequencies (Γ and W points), the damping is diminished in the vertex-neglected case. The vertex corrections predict that damping is maintained, even up to the largest energies. It is likely that the DMFA overestimates the phonon energy at $(\pi, 0)$. The full DCA with vertex corrections is necessary to obtain a very crisp change at the phonon frequency.

nuclei would have to be taken into account, and one would start with a momentum dependent dispersion [29]. In order to apply DCA to such a problem, one would have to apply a coarse graining procedure to the phonon self-energy, in a similar spirit to [24]. In case a realistic model induces a momentum dependent coupling constant, then additional coarse graining could be carried out as in [14]. This would lead to a smooth dispersion as in the electron case. It is clear that the complete softening of the (π, π) mode that is seen in the vertex neglected theory (top left) is absent in the vertex corrected theory (top right). One of the main effects of non-local fluctuations can be seen here, since the DCA predicts that electron-phonon coupling induces a dispersion in the Holstein model (absent in the DMFA). As shown here, the dispersion induced from the coupling of electrons to a single Einstein mode is similar to the effects of inter-nucleus coupling in a non-interacting system. This means that it could be quite difficult to distinguish between the two effects in the analysis of experimental data.

4.2. Electron dispersions and spectral functions

The quasi-particle dispersion and lifetime are important physical quantities that can be measured by the ARPES technique. The renormalised dispersion can be calculated

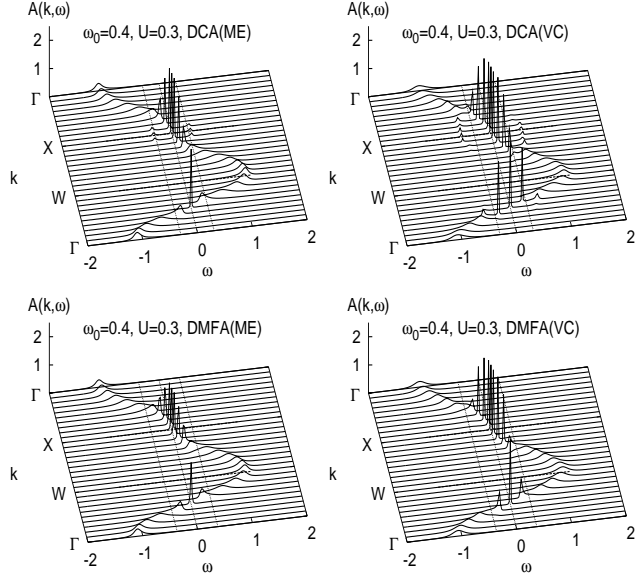


Figure 8. As figure 7, but with $U = 0.3$, $\omega_0 = 0.4$. In the case of the vertex corrected DCA, the quasi-particles are suddenly damped at the $(\pi, 0)$ phonon energy (shown by the parallel dotted lines). This sudden increase of damping is consistent with the experimental results in [2]. The vertex neglected theory consistently estimates the energy for the damping to begin at frequencies lower than the phonon frequency at the X point. As with figure (7), the vertex corrections maintain the damping up to the highest energies.

by solving the equation,

$$\omega + \mu - \epsilon_{\mathbf{k}} - \text{Re}[\Sigma(\omega, \mathbf{K})] = 0 \quad (12)$$

in analogy to the calculation of the phonon dispersion. Unlike the phonon calculations, the electron dispersion can be determined at all \mathbf{k} points, owing to the many to one mapping involved in coarse graining the self-energy. Here \mathbf{K} is the momentum of the coarse grained cell containing the momentum \mathbf{k} .

Figure 5 shows the electron dispersion of the Holstein model, for $U = 0.3$, $\omega_0 = 0.2$. The analytic continuation of the self energy was carried out using the maximum entropy method [25], since the normalisation of the spectral weight is known, and a reasonable default model can easily be constructed. The Padé approximant technique was not found to be very stable for the analytic continuation of self-energies. One reason for this may be that the self-energy has a high energy behaviour of $1/\omega$, whereas the bosonic propagators have $1/\omega^2$ behaviour, and therefore the contribution to the approximant from higher frequencies is smaller.

By examining the dispersions calculated for $\omega_0 = 0.2$ it can be seen that the main feature of the electron dispersion is a “kink” at the energy corresponding to the phonon frequency at the X point (the phonon frequency is marked as a horizontal dotted line). This is persistent for all the approximations. Vertex corrections stabilise the kink, and make it sharper. The kink is especially well defined along the $W-\Gamma$ line, where the

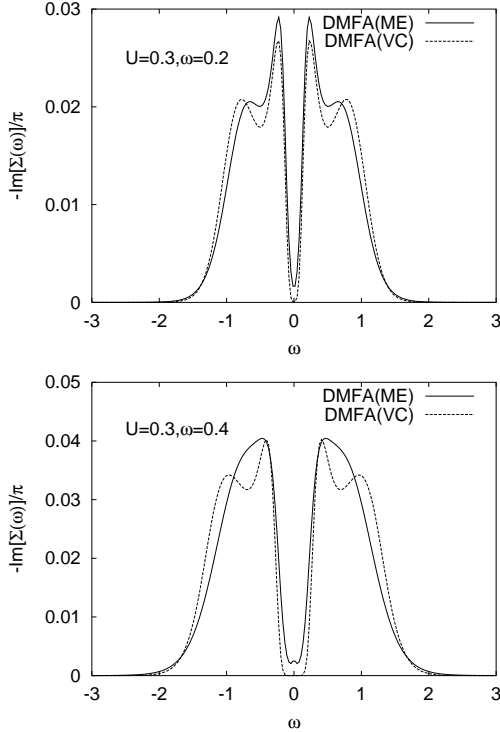


Figure 9. Self energy of the Holstein model approximated using the DMFA, with and without vertex corrections. Since the self-energy of the DCA varies in a complicated manner throughout the Brillouin zone, it is not shown here. As the vertex corrections act against the Fock term, and have a much lower energy scale, the quasi-particle damping at the Fermi energy is suppressed. However, the zeroth order moment is uniquely defined by the Fock term, and so the total normalisation must be conserved. This means that weight is shifted toward higher energies, leading to the suppression of quasi-particle states at the top of the dispersion.

4 approaches agree to reasonable accuracy. It is possible that the kink is located slightly below the renormalised phonon frequency in the dispersion calculated using the DMFA. Such a discrepancy is expected, since the renormalisation of the phonon frequency in DMFA is constant across the Brillouin zone, an assumption which is only true when phonon frequency and coupling are small as pointed out in section 4.1. The kink is not well defined along the Γ - X - W direction, unless the dispersion is calculated using the DCA(VC) scheme, where a sudden discontinuity is seen. The location of this discontinuity does not coincide with the boundary to a coarse grained cell, and is therefore not a result of the DCA. I note that some spurious dispersion is seen (small points). However, the quasi-particle weight of these points is small, and they are only included for completeness.

Figure 6 shows the electron dispersion for $U = 0.3$, $\omega_0 = 0.4$. Note that in the results from the DMFA calculations, the energy at which the kink occurs is significantly lower than the X -point phonon frequency. Results for the DCA(ME) bend smoothly, rather than kinking suddenly, at an energy scale, which may be slightly lower than the phonon frequency. Only the DCA(VC) has well defined kink behaviour along the W - Γ line. The discontinuity in the dispersion along the Γ - X - W line can also be seen

at this frequency. It is therefore quite clear that vertex corrections are significant for this set of parameters.

In order to calculate spectral functions at general \mathbf{k} , the coarse grained self energy is used in the following equation,

$$G(\omega, \mathbf{k}) = \frac{1}{\omega + i\eta + \mu - \epsilon_{\mathbf{k}} - \Sigma(\omega, \mathbf{K})} \quad (13)$$

where \mathbf{K} is the momentum point in the coarse graining cell which corresponds to \mathbf{k} .

In the calculation of the electron dispersion, some information is lost. For example, the quasi particle lifetime, which is related to the width of the peak in the spectral function cannot be seen. In order to demonstrate these effects, figure 7 shows a waterfall plot of spectral functions along the high symmetry directions for $U = 0.3$, $\omega_0 = 0.2$. The dotted lines running along the k axis represent the renormalised phonon frequency at the $(\pi, 0)$ point.

Sharply peaked points can be seen close to the Fermi-energy ($\omega = 0$), showing well defined quasi-particles. The quasi-particles are suddenly damped close to the renormalised phonon frequency corresponding to the $(\pi, 0)$ point, i.e. the peaks develop a width. At higher frequencies, the damping diminishes in the vertex neglected case and the peaks get higher and narrower. On the other hand, vertex corrections ensure that strong damping is maintained, even up to the largest energies. As discussed previously, it is thought that the DMFA overestimates the renormalised phonon frequency at $(\pi, 0)$. The full DCA with vertex corrections predicts a very crisp kink and reduction in the quasi-particle lifetime at the X -point phonon frequency.

Figure 8 also shows spectral functions but now with the larger phonon frequency, $\omega_0 = 0.4$. As with the $\omega_0 = 0.2$ results, the vertex-corrected DCA predicts a sudden damping of the quasi-particles at the $(\pi, 0)$ phonon energy. This sudden increase in damping connected with the kink is consistent with the photoemission experiment in [2]. The vertex neglected theory predicts a much lower energy for the damping to begin. One can see that the kink predicted by the DMFA begins at a lower energy than the phonon frequency, and (for the vertex corrected DMFA) that the damping changes smoothly, rather than suddenly before the phonon energy, although full damping is not seen until above the phonon energy.

The origin of the damping, and of the strong quasi-particles close to the Fermi-surface can be demonstrated by examining the self energy. Figure (9) shows the self energy of the Holstein model approximated using the DMFA, with and without vertex corrections. The self-energy of the DCA is not shown, since it varies throughout the Brillouin zone. The form of the DCA self-energies are similar. As the vertex corrections act to reduce the self-energy at low energy scales, the self energy at the Fermi energy is suppressed, leading to well defined quasi-particles at low energies. However, the high frequency behaviour is defined by the first-order term in the self energy, and this can be related to the normalisation of the self-energy spectrum. Therefore the total normalisation is seen to be conserved, regardless of the approximation used. If the weight of the self-energy is reduced at low frequencies, this weight must be shifted toward higher energies, leading to the suppression of quasi-particle states at the top of the dispersion.

5. Summary

In this paper, I applied the newly developed dynamical cluster approximation to the calculation of the electron dispersion, induced phonon dispersion, spectral functions

and phonon DOS for the Holstein model. A theory neglecting vertex corrections (related to Migdal–Eliashberg theory) and another incorporating the lowest order vertex correction were investigated. In contrast to previous work, non-local corrections were included. The application of DCA to this problem was crucial, since the double three-fold (four-fold including Matsubara summations) integration involved with the vertex corrected self-energy of phonons and electrons means that only small clusters can be considered, precluding finite size calculations.

The effect of non-local corrections to the vertex neglected theory of electron–phonon interactions is dramatic. Inclusion of non-local corrections to the theory results in a complete softening of the phonon modes at and close to the (π, π) point, which increases the effective coupling, λ . Therefore, a first-principles approach to the electron–phonon problem in two dimensions which neglects the effects of vertex corrections, but keeps the effects of non-local corrections, can only be applied to a very small range of phonon frequencies and couplings.

Vertex corrections act against the non-vertex corrected theory in both the phonon and electron self-energies. In the case of the phonon self-energy, which renormalises the phonon frequency, the correction acts to avert the complete softening of the mode. Therefore, λ is stabilised. The theory with vertex corrections also acts to stabilise the kink in the electron dispersion at large phonon frequencies, and causes an enhancement in the kink.

The results of this study have wide ranging implications for the application of Migdal–Eliashberg theory to the electron–phonon problem. Dispersion can be induced in the phonon modes, making it difficult to estimate the true coupling from fits to experimental data. Vertex corrections act to return the system to the Migdal parameter regime. Therefore, it is not surprising that the Migdal–Eliashberg theory has been so successful in describing the properties of a wide range of superconductors.

There is a large scope for extension to this work. The most direct and straightforward extensions would be to investigate the superconducting phase, the phase diagram and the 3D problem. It would also be interesting to study the effects of even higher-order vertex corrections. This is not practical within perturbation theory, since an implementation would involve many 3-fold integrations. An alternative method for including vertex corrections would be to employ a quantum Monte-Carlo simulation. Such work is currently in progress.

Acknowledgments

JPH would like to acknowledge support from the Guest Scientist program of the Max-Planck-Institute für Physik Komplexer Systeme, and useful discussions with Mark Jarrell, Jim Freericks, Nick d’Ambrumenil and Emma Chung.

- [1] G.M.Zhao, K.Conder, H.Keller, and K.A.Müller. *Nature*, 381:676, 1996.
- [2] A.Lanzara, P.V.Bogdanov, X.J.Zhou, S.A.Kellar, D.L.Feng, E.D.Lu, T.Yoshida, H.Eisaki, A.Fujimori, K.Kishio, J.-I.Shimoyama, T.Noda, S.Uchida, Z.Hussa, and Z.-X.Shen. *Nature*, 412:6846, 2001.
- [3] R.J.McQueeney, Y.Petrov, T.Egami, M.Yethiraj, G.Shirane, and Y.Endoh. *Phys. Rev. Lett.*, 82:628, 1999.
- [4] J.K.freericks, V.Zlatic, W.Chung, and M.Jarrell. Vertex-corrected perturbation theory for the electron–phonon problem with non-constant density of states. *Phys. Rev. B*, 58:11613, 1998.
- [5] A.B.Migdal. 7:996, 1958.

- [6] G.M.Eliashberg. Interactions between electrons and lattice vibrations in a superconductor. 11:696, 1960.
- [7] M.Grabowski and L.J.Sham. Superconductivity from nonphonon interactions. *Phys. Rev. B*, 29:6132, 1984.
- [8] V.N.Kostur and B.Mitrović. Electron-phonon interaction in two dimensions: Variation of $\text{im}\sigma(\epsilon_p, \omega)$ with increasing ω_d/e_f . *Phys. Rev. B*, 48:16388, 1993.
- [9] C.Grimaldi, L.Pietrono, and S.Strässler. Nonadiabatic superconductivity: Electron-phonon interaction beyond migdal's theorem. *Phys. Rev. Lett.*, 75:1158, 1995.
- [10] O.V.Danylenko and O.V.Dolgov. Nonadiabatic contribution to the quasiparticle self-energy in systems with strong electron-phonon interaction. *Phys. Rev. B*, 63:094506, 2001.
- [11] P.Miller, J.K.Freericks, and E.J.Nicol. Possible experimentally observable effects of vertex corrections in superconductors. *Phys. Rev. B*, 58(21):14498, 1998.
- [12] A.Deppeler and A.J.Millis. Dynamical mean-field theory of electron-phonon interactions in correlated systems: Application to isotope effects on electronic properties. *Phys. Rev. B*, 65:224301, 2002.
- [13] M.Hettler, A.N.Tahvildar-Zadeh, M.Jarrell, T.Pruschke, and H.R.Krishnamurthy. Nonlocal dynamical correlations of strongly interacting electron systems. *Phys. Rev. B*, 58:7475, 1998.
- [14] M.Hettler, M.Mukherjee, M.Jarrell, and H.R.Krishnamurthy. *Phys. Rev. B*, 61:12739, 2000.
- [15] W.Metzner and D.Vollhardt. *Phys. Rev. Lett.*, 62:324, 1989.
- [16] A.Georges, G.Kotliar, W.Krauth, and M.Rozenburg. *Rev. Mod. Phys.*, 68:13, 1996.
- [17] A.N.Tahvildar-Zadeh, J.K.Freericks, and M.Jarrell. Magnetic phase diagram of the hubbard model in three dimensions: the second-order local approximation. *Phys. Rev. B*, 55:942, 1997.
- [18] M.Jarrell, Th.Maier, C.Huscroft, and S.Moukouri. A quantum monte carlo algorithm for non-local corrections to the dynamical mean-field approximation. *Phys. Rev. B*, 2001.
- [19] T.Hahn, editor. *International tables for crystallography. Volume A: Space group symmetry*. Kluwer Academic Publishers, Dordrecht, 1996.
- [20] Ph.Lambin and J.P.Vigneron. Computation of crystal green's functions in the complex-energy plane with the use of the analytical tetrahedron method. *Phys. Rev. B*, 29:3430, 1984.
- [21] T.Holstein. *Ann. Phys.*, 8:325–342, 1959.
- [22] N.E.Bickers and D.J.Scalapino. *Ann. Phys.*, 193:206, 1989.
- [23] A.J.Millis, R.Mueller, and B.I.Shraiman. Fermi-liquid-to-polaron crossover. i. general results. *Phys. Rev. B*, 54:5389, 1996.
- [24] Y.Motome and G.Kotliar. Effects of boson dispersion in fermion-boson coupled systems. *Phys. Rev. B*, 62:12800, 2000.
- [25] M.Jarrell and J.E.Gubernatis. Bayesian inference and the analytic continuation of imaginary-time monte carlo data. *Physics Reports*, 269:135, 1996.
- [26] H.J.Vidberg and J.W.Serene. *J. Low Temp. Phys.*, 29:179, 1977.
- [27] J.P.Carbonne. Properties of boson-exchange superconductors. *Rev. Mod. Phys.*, 62:1027, 1990.
- [28] H.A.Mook, B.C.Chakoumakos, M.Mostoller, A.T.Boothroyd, and D.McK.Paul. *Phys. Rev. Lett.*, 69:2272, 1992.
- [29] N.W.Ashcroft and N.D.Mermin. *Solid State Physics*. Saunders, Philadelphia, 1975.